

Orbital properties of an unusually low-mass sdB star in a close binary system with a white dwarf

R. Silvotti^{1*}, R. H. Østensen², S. Bloemen², J. H. Telting³, U. Heber⁴, R. Oreiro⁵,
M. D. Reed⁶, L. E. Farris⁶, S. J. O’Toole⁷, L. Lanteri¹, P. Degroote², H. Hu⁸,
A. S. Baran^{6,9}, J. J. Hermes¹⁰, L. G. Althaus¹¹, T. R. Marsh¹², S. Charpinet¹³, J. Li¹⁴,
R. L. Morris¹⁴, D. T. Sanderfer¹⁴

¹ INAF-Osservatorio Astrofisico di Torino, Strada dell’Osservatorio 20, 10025 Pino Torinese, Italy

² Instituut voor Sterrenkunde, KU Leuven, Celestijnenlaan 200D, 3001 Leuven, Belgium

³ Nordic Optical Telescope, Apartado 474, 38700 Santa Cruz de La Palma, Spain

⁴ Dr. Karl Remeis-Observatory & ECAP, Astronomical Inst., FAU Erlangen-Nuremberg, Sternwartstr. 7, 96049 Bamberg, Germany

⁵ Instituto de Astrofísica de Andalucía, Glorieta de la Astronomía s/n, 18008 Granada, Spain

⁶ Department of Physics, Astronomy and Materials Science, Missouri State University, Springfield, MO 65897, USA

⁷ Anglo-Australian Observatory, PO Box 296, Epping, NSW 1710, Australia

⁸ Institute of Astronomy, The Observatories, Madingley Road, Cambridge CB3 0HA, UK

⁹ Uniwersytet Pedagogiczny, Obserwatorium na Suhorze, ul. Podchorążych 2, 30-084 Kraków, Polska

¹⁰ Department of Astronomy, University of Texas at Austin, Austin, TX 78712, USA

¹¹ Facultad de Ciencias Astronómicas y Geofísicas, Universidad Nacional de La Plata, La Plata 1900, Argentina

¹² Department of Physics, University of Warwick, Coventry CV4 7AL, UK

¹³ Laboratoire d’Astrophysique de Toulouse-Tarbes, Université de Toulouse, 14 avenue Edouard Belin, Toulouse 31400, France

¹⁴ SETI Institute/NASA Ames Research Center, Moffett Field, CA 94035, USA

Released 2012 Xxxxx XX

ABSTRACT

We have used 605 days of photometric data from the *Kepler* spacecraft to study KIC 6614501, a close binary system with an orbital period of 0.15749747(25) days (3.779939 hours), that consists of a low-mass subdwarf B (sdB) star and a white dwarf. As seen in many other similar systems, the gravitational field of the white dwarf produces an ellipsoidal deformation of the sdB which appears in the light curve as a modulation at two times the orbital frequency. The ellipsoidal deformation of the sdB implies that the system has a maximum inclination of ~ 40 degrees, with $i \approx 20^\circ$ being the most likely. The orbital radial velocity of the sdB star is high enough to produce a Doppler beaming effect with an amplitude of 432 ± 5 ppm, clearly visible in the folded light curve. The photometric amplitude that we obtain, $K_1 = 85.8$ km/s, is ~ 12 per cent less than the spectroscopic RV amplitude of 97.2 ± 2.0 km/s. The discrepancy is due to the photometric contamination from a close object at about 5 arcsec North West of KIC 6614501, which is difficult to remove. The atmospheric parameters of the sdB star, $T_{\text{eff}} = 23\,700 \pm 500$ K and $\log g = 5.70 \pm 0.10$, imply that it is a rare object below the Extreme Horizontal Branch (EHB), similar to HD 188112 (Heber et al. 2003). The comparison with different evolutionary tracks suggests a mass between ~ 0.18 and $\sim 0.25 M_\odot$, too low to sustain core helium burning. If the mass was close to 0.18 – $0.19 M_\odot$, the star could be already on the final He-core WD cooling track. A higher mass, up to $\sim 0.25 M_\odot$, would be compatible with a He-core WD progenitor undergoing a cooling phase in a H-shell flash loop. A third possibility, with a mass between ~ 0.32 and $\sim 0.40 M_\odot$, can not be excluded and would imply that the sdB is a “normal” (but with an unusually low mass) EHB star burning He in its core. In all these different scenarios the system is expected to merge in less than 3.1 Gyr due to gravitational wave radiation.

Key words: binaries: close – hot subdwarfs – white dwarfs – stars: individual: KIC 6614501

1 INTRODUCTION

Hot subdwarf stars (sdBs and sdOs) are found in all galactic stellar populations and they are the main source of the UV-upturn phenomenon in early-type galaxies (Greggio & Renzini 1990; Brown et al. 1997). Subdwarf B stars in particular are post red giant branch (RGB) stars with thin ($\lesssim 0.01 M_{\odot}$) inert hydrogen envelopes. Most of them have masses close to $0.5 M_{\odot}$, with a peak near 0.47, and are core helium-burning objects on the extreme horizontal branch (EHB). If the mass of an sdB star is below $\sim 0.3 M_{\odot}$, the He-core ignition never took place. These rare stars are the progenitors of He-core white dwarfs. A recent extensive review on sdB/sdO stars is given by Heber (2009).

In order to reach the high temperatures and surface gravities typical of sdB stars, their progenitors must have lost almost the entire hydrogen envelope near the tip of the red giant branch (RGB). This may happen in a close binary after a common-envelope (CE) phase, when the orbital angular momentum is transferred to the red giant envelope spinning up the envelope until enough energy has been accumulated to eject it. Indeed, about half of sdBs reside in close binary systems with white dwarfs (WDs) or low-mass main-sequence stars (Maxted et al. 2001; Napiwotzki et al. 2004). The various formation channels of sdB stars have been studied by Han et al. (2002, 2003).

Presently, more than one hundred close binaries with an sdB component are known (Geier et al. 2011a,b; Copperwheat et al. 2011), and an important fraction must be composed by sdB+WD binaries. These systems are potential progenitors of type Ia supernovae (SN), provided that the total mass exceeds the Chandrasekhar limit and that the initial separation is small enough to merge in a Hubble time due to gravitational wave radiation. The first candidate found to be a type Ia SN progenitor is KPD 1930+2752 (Maxted et al. 2000; Geier et al. 2007), with a total mass of $1.47 M_{\odot}$ when we assume a canonical value of $0.5 M_{\odot}$ for the sdB component. Another interesting sdB+WD system, KPD 1946+4340, was observed by the *Kepler* spacecraft and studied in great detail (Bloemen et al. 2011). Thanks to its brightness ($V=14.28$) and high inclination (87.1°), KPD 1946+4340 shows very clean primary and secondary eclipses and a very accurate light curve modelling was possible, including not only ellipsoidal deformation and Doppler beaming, but also WD reflection and gravitational lensing.

The target discussed in this article, KIC 6614501 (alias 2MASS J19365001+4201436), is another such sdB+WD system. It was selected among a list of sdB pulsator candidates inside the *Kepler* field of view, with the main goal of performing detailed asteroseismic studies of these stars. During the *survey phase* (Østensen et al. 2010b, 2011), it was observed by the *Kepler* space telescope (Borucki et al. 2010) in the framework of the *Kepler* Asteroseismic Science Consortium (Gilliland et al. 2010). The first results after 1 month of observation are reported by Østensen et al. (2011): no pulsations were detected and the atmospheric parameters were determined from spectroscopy at the 4.2 m William Herschel Telescope. A low frequency modulation plus its 1st harmonic in the *Kepler* light curve was interpreted as a binary signature, suggesting a sdB+WD system because no red excess was seen in the spectrum of the star. Østensen et al. (2011) also noted the peculiar position of KIC 6614501 in the $T_{\text{eff}}/\log g$ plane, below the EHB, implying a low-mass post-RGB object. A mass of about $0.24 M_{\odot}$ was suggested by comparing its position with the evolutionary tracks of Driebe et al. (1998), implying that KIC 6614501 could evolve into a He-core white dwarf.

This particular configuration may occur when the envelope of

the red giant is ejected before the core has attained sufficient mass to ignite helium. In this case, the RG core may cross the region of the EHB stars near its low temperature - low gravity edge, before evolving to the WD cooling track. These post-RGB low-mass objects are rare and only recently their number has increased significantly thanks in particular to the results of the ELM=Extreme Low Mass (WD) survey (Brown et al. 2010), the *Kepler* mission, and the WASP (Wide Angle Search for Planets) survey (e.g. Maxted et al. 2011). The ELM survey has found many new double degenerate systems, increasing the number of those previously discovered by the SPY survey (Koester et al. 2009). A spectacular case is J1741+6526, composed by a ELM WD primary of $0.16 M_{\odot}$ and an unseen companion with a minimum mass of $1.1 M_{\odot}$: with an orbital period of 1.47 hours, it should merge in less than 170 Myr. Assuming an inclination of 60 degrees, the total mass would be $1.7 M_{\odot}$ (Brown et al. 2012).

However, most ELM WDs are concentrated at effective temperatures below 15 000 K. At higher temperatures, the number of known ELM WDs (or ELM WD precursors) is very small, with only a few candidates. KIC 6614501 is the hottest candidate in a region of the $T_{\text{eff}}/\log g$ plane almost completely empty and crucial to understand the evolution of the stars that have a mass close to the limit for He-core burning. The system most similar to KIC 6614501 is HD 188112, with a $\sim 0.24 M_{\odot}$ sdB primary and a massive ($>0.73 M_{\odot}$) unseen companion (Heber et al. 2003). If the companion was a C/O WD with a mass larger than $0.9 M_{\odot}$, HD 188112 would be the precursor of a subluminal SN Ia.

In the next sections we will perform a detailed study of the properties of KIC 6614501, based on *Kepler* data plus spectroscopic follow-up. In the last section of this article, our results are placed in the context of the ELM white dwarfs.

2 KEPLER LIGHT CURVE AND EPHEMERIS

KIC 6614501 was observed by *Kepler* in short cadence (SC, 59 s sampling) during the following monthly runs (“Q” stands for quarter): Q3.3, Q5.1, Q5.2, Q5.3, Q6.1, Q6.2, Q6.3, Q8.1, Q8.2, Q8.3, Q9.1, Q9.2, Q9.3, Q10.1, Q10.2 and Q10.3 for a total duration of 458.9 days. Moreover it was observed in long cadence (LC, 29.4 min sampling) during Q3.1, Q3.2 and Q7 (146.4 days in total). The data were downloaded from the *Kepler* Asteroseismic Science Operations Center (KASOC) website¹. The data files contain Barycentric Julian Dates (BJD), raw fluxes with errors, and corrected fluxes with errors. The corrected fluxes are computed by estimating and subtracting the contamination by close objects, based on their spectral energy distribution. However, the colour-based atmospheric parameters (T_{eff} and $\log g$) of the stars in the *Kepler* database are not accurate for stars with peculiar properties such as very hot stars. For this reason we decided to use raw fluxes. This choice may affect the relative amplitude of the orbital modulation and its 1st harmonic: a discussion of this aspect is given in section 4.1.

For each run the fluxes were corrected for long-term trends using a cubic spline interpolation or a straight line in a few cases. We removed outliers ($>4 \times$ standard deviation), and the fluxes were divided by their mean value in order to normalize all runs to an average value of 1.

¹ <http://kasoc.phys.au.dk/kasoc/>

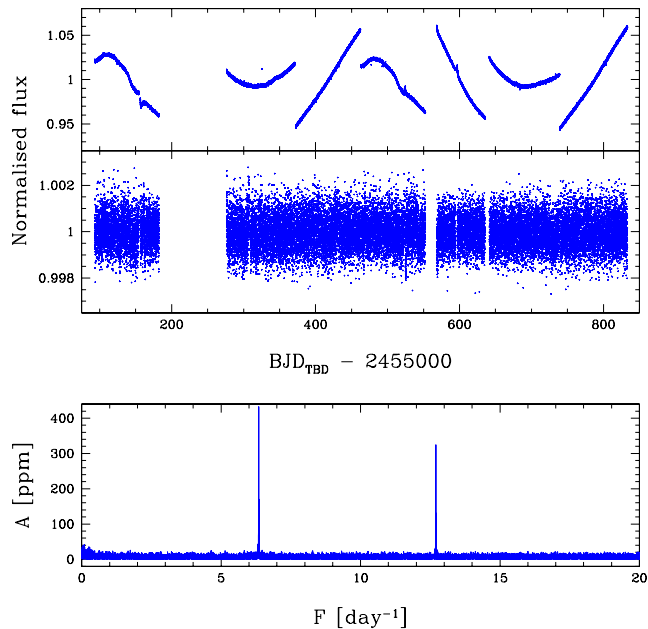


Figure 1. Top: the *Kepler* raw light curve after normalisation of each segment (upper panel) and after cubic spline (or straight line) correction (middle panel). Bottom: amplitude spectrum at low frequency showing the orbital period and its first harmonic. Only in the two upper panels, in order to reduce the size of the figures, we used a light curve with a reduced number of points by binning to 29.4 min all the short cadence data (while in the lower panel and in all our analysis the data were used with their original sampling time).

A first Fourier analysis up to the Nyquist frequency was performed using only the short cadence data to check for any possible presence of high-frequency oscillations. Excluding some known artifacts, only a few peaks were found with an amplitude just beyond the threshold which we fixed at 4 times the mean value of the amplitude spectrum (4σ). The highest peak is at 579.319 d^{-1} ($670.508 \mu\text{Hz}$), with an amplitude of 28.9 ppm, corresponding to 4.3σ . With more data from *Kepler* it will be possible in the future to confirm or not the presence of high-frequency oscillations in KIC 6614501.

The low-frequency analysis was done using all the 676 744 data points (SC + LC), keeping their original sampling time. We verified that the smearing effect introduced by LC data was smaller than the amplitude uncertainty. At low frequency, the Fourier amplitude spectrum shows two peaks that correspond to the orbital period and its first harmonic. The latter is the result of the ellipsoidal deformation of the sdB star due to the gravitational field produced by the companion. Less obvious is the correct interpretation of the orbital modulation, which requires also the phase information (see section 4). The light curve and the amplitude spectrum at low frequency are shown in Fig. 1.

From fitting the orbital period to the *Kepler* light curve, we obtain the following ephemeris:

$$\text{BJD}_{\text{TDB}} = 2455093.33296(31) + 0.15749747(25) E$$

which gives the times when the sdB is closest to the Earth (i.e. phase 0 in Fig. 4). The reference epoch corresponds to the first time at phase 0 of the *Kepler* data.

3 SPECTROSCOPY

On the nights of 12 and 15 August 2010 we obtained 22 spectra of KIC 6614501 with the Kitt Peak National Observatory (KPNO) 4-m Mayall telescope and its RC-Spec/F3KB spectrograph. The spectra cover the H_{β} – H_{η} region with a dispersion of $0.45 \text{ \AA}/\text{pix}$ and a resolution of 1.6 \AA . The exposure time was 600 seconds, yielding a median $S/N=38$ per pixel.

Similarly, on the night of 27 June 2010, we obtained 10 spectra at the 2.5-m Isaac Newton Telescope (INT) with the IDS235+EEV10 spectrograph, with a resolution of 3.0 \AA , exposure time of 1600 seconds, and median $S/N=42$ when resampled to the KPNO 4m dispersion.

The data were homogeneously reduced and analysed. Standard reduction steps within IRAF² were: bias subtraction, removal of pixel-to-pixel sensitivity variations, optimal spectral extraction, and wavelength calibration based on arc lamp spectra. The target spectra and mid-exposure times were shifted to the barycentric frame of the solar system. The spectra were normalised to place the continuum at unity by comparing with a model spectrum for a star with similar physical parameters as we find for the target (see section 3.2).

3.1 Spectroscopic radial velocities

Radial velocities (RVs) were derived with the FXCOR package in IRAF using the H_{β} , H_{γ} , H_{ζ} and H_{η} lines. All the RV measurements are reported in Table 1. Fits assuming a sinusoidal orbital velocity curve confirm the orbital period as $0.157497(5) \text{ d}$, fully consistent with the photometric orbital period found from the *Kepler* data. The RV amplitude that we find is $97.2 \pm 2.0 \text{ km/s}$. Due to the relatively long exposure times of the INT data, the measured velocities are smeared-out to result in an RV amplitude that is lower than the fit by about 2 km/s . For the KPNO data the smearing effects due to the exposure time are negligible. When fitting the data of each observatory with the period and phase fixed from the all-data fit, we found that the RV amplitude is consistent. The system velocity is $-9.9(2.2) \text{ km/s}$ for the KPNO data, and $0.5(3.2) \text{ km/s}$ for the INT data. This zero point offset also shows up in the position of the interstellar CaII 3993 \AA line in the mean spectrum of each telescope. Although the measurements of the position of this line are not accurate enough to calibrate this offset, it is clear that the offset is site dependent and does not imply the presence of a third body. Our best fit is shown in Fig. 2 and the fit parameters are listed in Table 2. The orbital period was fixed to the value determined from *Kepler* photometry.

After the orbital fits, the spectra were shifted to remove the orbital motion, before being co-added to obtain high S/N spectra ($S/N \sim 150$) with minimal orbital line broadening, for both observatories. These spectra were used to derive the atmospheric parameters of the star.

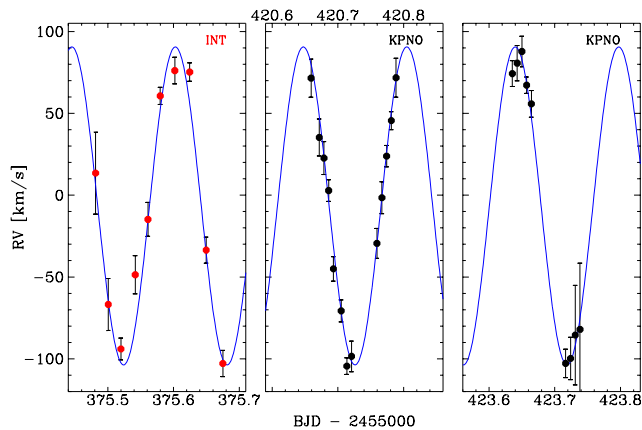
3.2 Improved atmospheric parameters

The high S/N mean spectra from the INT and KPNO, shown in Fig. 3, were fitted to a grid of LTE spectra computed *ad hoc* for this star (Heber et al. 2000). Since there is no detectable helium lines

² Image Reduction and Analysis Facility, written and supported by the National Optical Astronomy Observatories (NOAO) in Tucson, Arizona (<http://iraf.noao.edu/>).

Table 1. RV measurements.

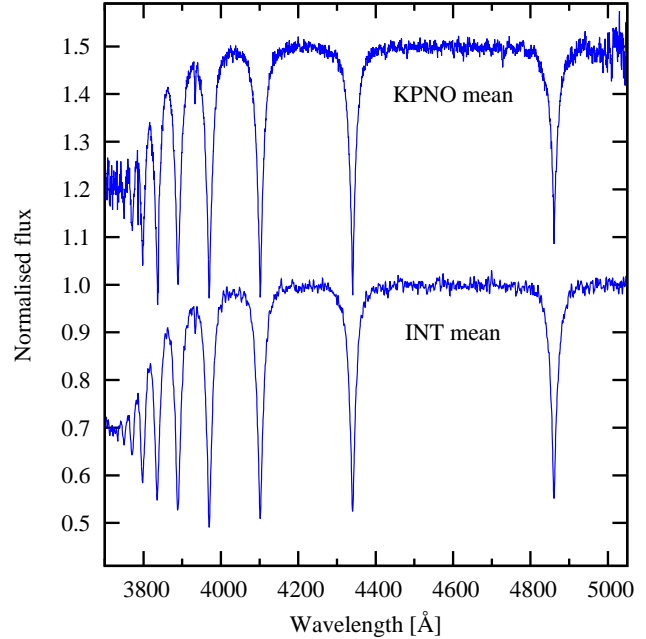
BJD	v (km/s)	error (km/s)
2455375.481497	13.5	25.0
2455375.500704	-66.8	15.9
2455375.520005	-94.0	6.6
2455375.541801	-48.6	11.7
2455375.561105	-14.8	10.4
2455375.579773	60.7	5.3
2455375.601982	76.1	8.1
2455375.624646	75.2	5.7
2455375.649749	-33.6	8.0
2455375.675079	-102.8	8.0
2455420.659287	71.5	11.6
2455420.671652	35.3	11.3
2455420.678830	22.7	10.1
2455420.685997	2.8	6.6
2455420.693178	-45.0	7.5
2455420.705115	-70.7	6.8
2455420.713657	-104.5	5.0
2455420.720826	-98.5	9.4
2455420.759432	-29.5	9.2
2455420.766993	-1.5	9.7
2455420.774178	23.9	6.6
2455420.781347	45.6	5.5
2455420.788526	71.8	11.9
2455423.635478	74.3	7.9
2455423.642873	80.7	10.8
2455423.650043	87.8	9.4
2455423.657195	67.2	5.0
2455423.664441	55.8	8.2
2455423.716534	-102.8	8.7
2455423.724074	-99.8	12.9
2455423.731241	-85.5	30.4
2455423.738429	-82.0	40.5

**Figure 2.** The radial velocity curve of KIC 6614501 using the orbital period as determined from *Kepler* photometry. See the text for more details.

in the spectra, we fixed the helium abundance to $\log(N_{\text{He}}/N_{\text{H}}) = -3.0$. The grids were computed at solar metallicity and at metallicities reduced by a factor of 10 or 100 relative to solar composition. From an evaluation of the line strength in the models when convolved with the instrumental profile, we infer, from the non-detection of any metal features in our spectra, that the overall metallicity must be significantly sub-solar, at least $\log[Z] < -1.5$. But

Table 2. Orbital fit parameters using the orbital period from *Kepler* photometry.

Offset (km/s)	-6.5 ± 1.5
Amplitude (km/s)	97.2 ± 2.0
Period (day)	0.15749747
Phase 0 (BJD-2455000)	375.56366 ± 0.00054
χ^2_{red}	1.58

**Figure 3.** The high S/N mean spectra from the INT and KPNO.

we know that individual elements may be substantially under- or overabundant relative to the solar composition, as is typical for the sdB stars due to the competing effects of gravitational settling and radiative levitation and to possible radiation-driven wind (see section 5 of Heber 2009 and references therein). In the end we decided to use the grid computed at $\log[Z] = -2.0$ for the final analysis. The H_{β} line was kept out of the fit, partly due to a problem with the background subtraction in the KPNO data, and partly due to concerns regarding NLTE effects in the core, which are not accounted for by our models. For the KPNO data set the H_{η} line was also kept out due to a bad CCD column which translates into a broad artifact feature in the mean spectrum after applying the orbit correction. Our best atmospheric parameters from INT and KPNO spectra are summarised in Table 3.

Table 3. Best atmospheric parameters from INT and KPNO spectra.

Data	T_{eff}	$\log(g)$
INT	24 084[65]	5.732[11]
KPNO	23 332[80]	5.653[12]
Adopted	$23\,700 \pm 500$	5.70 ± 0.1

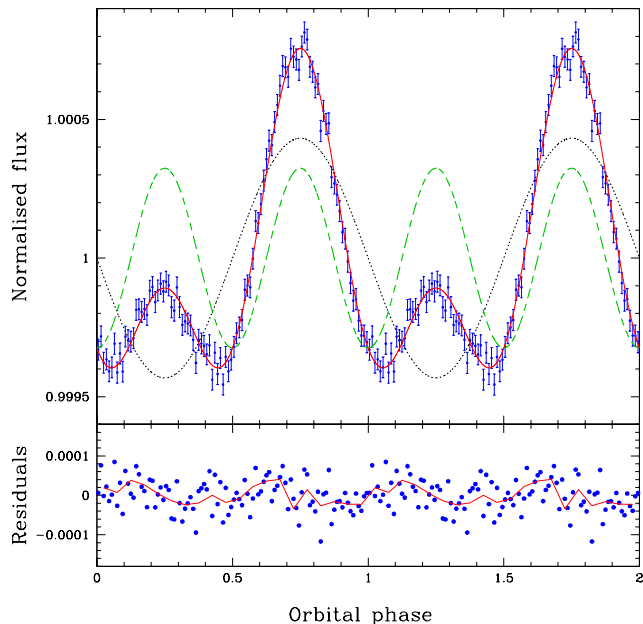


Figure 4. Phase-folded light curve of KIC 6614501 (data points grouped in 100 phase intervals) and our best fit, obtained considering two components: an orbital modulation that accounts for the beaming effect (black dotted) and an ellipsoidal modulation at twice the orbital frequency (green dashed). The bottom panel shows the residuals grouped in 100 (blue dots) and 20 (red line) phase intervals. Colors are available only in the electronic version.

4 LIGHT CURVE ANALYSIS

The light curve of KIC 6614501 can be fit using two components: the ellipsoidal deformation of the sdB star and the Doppler beaming. Our best fit to the data with two sinusoidal components is shown in Fig. 4. We obtain $\chi^2_{red} = 1.17$. The amplitudes of the orbital beaming frequency and of the ellipsoidal modulation at two times the orbital frequency are 432.4 ± 5.3 and 324.8 ± 5.3 ppm respectively. A third component due to the reflection effect by the illuminated hemisphere of the companion is too faint to be seen in the light curve and can be neglected. This component would have the maximum at phase 0.5 and is not seen in the residuals (bottom panel of Fig. 4). The lack of an observable reflection effect suggests that the companion must be a white dwarf. With such a short orbital period, an M-dwarf companion would be easily seen (see e.g. the folded light curves of KIC 1868650, KIC 9472174 (Østensen et al. 2010a,b), KIC 2991403, KIC 11179657 (Kawaler et al. 2010) and KIC 7335517 (Østensen et al. 2011)).

4.1 Doppler beaming and photometric RVs

The asymmetry in the ellipsoidal modulation of KIC 6614501 is caused by Doppler beaming (Hills & Dale 1974; Loeb & Gaudi 2003).

Doppler beaming, also called Doppler boosting, was first detected by Maxted et al. (2000) in the sdB+WD binary KPD 1930+2752. Recent detections of Doppler beaming are reported by Shporer et al. (2010) and Vennes et al. (2011), using data from the ground, and by Mazeh & Faigler (2010), who have measured the Doppler beaming caused by a substellar companion in CoRoT data. In the context of *Kepler*, Doppler beaming

was discussed by Loeb & Gaudi (2003) and Zucker et al. (2007). Thanks to *Kepler*'s sensitivity, van Kerkwijk et al. (2010) have obtained the first photometric radial velocities (RVs) for the two A/B+WD systems KOI 74 and KOI 81. For KOI 74 the photometric RVs were confirmed a-posteriori by spectroscopic measurements (Bloemen et al. 2012). A good agreement between photometric and spectroscopic RVs was found also for the two sdB+WD binaries KPD 1946+4340 (Bloemen et al. 2011) and KIC 11558725 (Telting et al. 2012).

When a source moves at a radial nonrelativistic speed v_r with respect to an observer, the observed flux F_λ is given by:

$$F_\lambda = F_{0\lambda} \left(1 - B_\lambda \frac{v_r}{c} \right) \quad (1)$$

where $F_{0\lambda}$ is the emitted flux and c is the light speed. $B_\lambda = B_g + B_{s\lambda} = 3 + (2 + d \ln F_\lambda / d \ln \lambda) = 5 + d \ln F_\lambda / d \ln \lambda$ is the beaming factor (Loeb & Gaudi 2003; Bloemen et al. 2011), which incorporates two different terms: a geometrical term $B_g = 3$, not depending on wavelength, that includes a +1 contribution (enhanced photon arrival rate of an approaching source) and a +2 contribution (solid angle geometrical aberration). And the Doppler shift $B_{s\lambda}$ that can either increase or decrease the flux of an approaching source, depending on its spectral energy distribution (SED) and on the instrumental bandpass. In our case, for a hot star, the optical flux is on the Rayleigh-Jeans tail of the distribution and therefore, when the star is approaching, the blue-shift pushes part of the flux outside the visibility range giving a negative contribution to the beaming factor.

When equation (1) is used in broadband photometry, we need to compute a weighted mean of the beaming factor that takes into account the star's SED and the bandpass, which in turn depends on the instrumental response function ($\epsilon_{i\lambda}$), atmospheric transmission ($\epsilon_{a\lambda}$) and interstellar medium transmission ($\epsilon_{im\lambda}$):

$$\langle B \rangle = \frac{\int \epsilon_{i\lambda} \epsilon_{a\lambda} \epsilon_{im\lambda} \lambda F_\lambda B_\lambda d\lambda}{\int \epsilon_{i\lambda} \epsilon_{a\lambda} \epsilon_{im\lambda} \lambda F_\lambda d\lambda} \quad (2)$$

In our case $\epsilon_{i\lambda}$ is the response function of the *Kepler* bandpass, $\epsilon_{a\lambda} \equiv 1$ at any λ , and $\epsilon_{im\lambda}$ is the interstellar medium transmission corresponding to a reddening $E(B - V) = 0.06 \pm 0.03$ mag (95% confidence interval). This value was obtained by collecting multi-colour photometry from the Carlsberg Meridian Catalog (SDSS r' band, ViZieR catalog I/304), the *Kepler* Input Catalog (SDSS g,r,i and z bands, ViZieR catalog V/133) and the UVEX survey (UVEX u, g, r, i and H α bands, Groot et al. 2009), and by following the method described in Degroote et al. (2011), but applied to a grid of sdB spectral energy distributions.

In order to compute the beaming factor and its uncertainty from equation (2), we have used a grid of fully metal line-blanketed LTE atmosphere models for sdB stars (Heber et al. 2000) with T_{eff} ranging from 21 000 to 25 000 K, $\log g$ between 5.1 and 5.9, metallicity between solar and 1/100 solar and fixed helium abundance $\log(N_{\text{He}}/N_{\text{H}}) = -3$. The beaming factor is found to be $\langle B \rangle = 1.51 \pm 0.02$ (1.52 without considering reddening). This value corresponds to a metallicity of 1/100 solar. The uncertainty incorporates any value of the metallicity between 1/100 solar and solar (metallicity is the main source of error), and an uncertainty of ± 500 K and ± 0.1 dex on the sdB's effective temperature and gravity.

Once the beaming factor is computed, in order to calculate the photometric radial velocity amplitude, equation (1) can be written as:

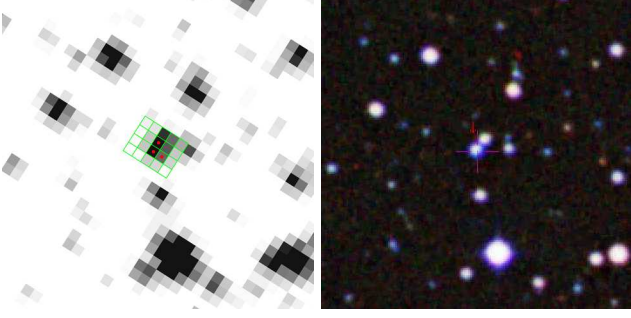


Figure 5. Left: the field of KIC 6614501 in a real *Kepler* image with the position of the pixel array mask used during the Q7 run. The pixel size of about 3.98 arcsec is not constant over time, differential velocity aberration results in the coordinates of the pixel mask changing constantly, typically by a few arcsec over each quarter. The three pixels actually used to form the optimal aperture, i.e. to collect photons from KIC 6614501, are those with a red dot (colors available only in the electronic version). Right: the same field in a SuperCosmos Sky Survey 3-color BRI image, which shows the target and its close companion at about 5.0 arcsec North West of it. Both images are $2' \times 2'$.

$$K = \frac{c A_B}{\langle B \rangle} \quad (3)$$

where A_B is the beaming amplitude. From equation (3) we obtain a photometric RV amplitude $K_1 = 85.8$ km/s, 11.7% less than the spectroscopic RV amplitude of 97.2 ± 2.0 km/s. The reason of this discrepancy is the photometric contamination from a close object, at approximately 5.0 arcsec North West of KIC 6614501, while the *Kepler*'s pixel size is 3.98 arcsec (see Fig. 5). This flux excess dilutes the beaming modulation and decreases its amplitude³. The uncertainty on the photometric RV amplitude is dominated by a systematic error given by the photometric contamination, which is difficult to estimate. Then we have two statistical errors associated with the beaming factor ($\pm 1.3\%$) and to the beaming amplitude ($\pm 1.2\%$), coming from the fit of the light curve.

4.2 Amplitude of the ellipsoidal deformation

From the comparison between photometric and spectroscopic RV amplitude, we have seen that only 88.3% of the photons attributed to KIC 6614501 actually come from this source. This means that not only the beaming amplitude but also the ellipsoidal modulation amplitude is reduced by the same amount. Thus we estimate that the amplitude of the ellipsoidal deformation, after correction for the photometric contamination, is 368.0 ± 11.7 ppm.

5 PROPERTIES OF THE BINARY SYSTEM

The binary system is described by the mass function, that can be expressed as follows:

$$\sin i = K_1 \left(\frac{P}{2\pi G} \right)^{1/3} \frac{(M_1 + M_2)^{2/3}}{M_2} \quad (4)$$

³ Even using the *Kepler* pixel data it is not possible to exclude the photons coming from the close source in a reliable way because the coordinates of the pixel mask change constantly in time, see caption of Fig. 5.

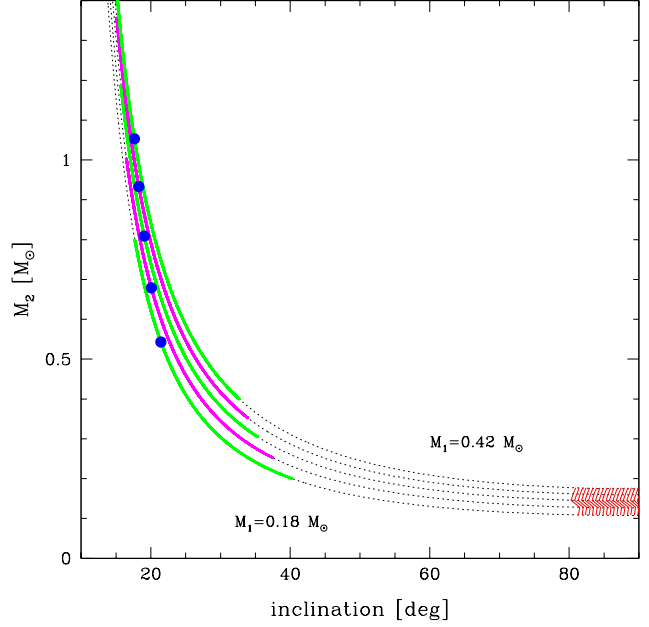


Figure 6. Mass of the white dwarf secondary as a function of the system's inclination for a wide range of sdB masses, from 0.18 to $0.42 M_\odot$ with $0.06 M_\odot$ steps. The red region on the right is forbidden by the lack of eclipses. When we consider also the amplitude of the ellipsoidal deformation of the sdB primary, we obtain a family of solutions represented by the blue dots and the green or violet 1σ uncertainties (colors available only in the electronic version). See text for more details.

In Fig. 6 the mass of the secondary⁴ is shown as a function of the system's inclination for a wide range of sdB masses. We see that the mass of the secondary is always larger than $\sim 0.1 M_\odot$.

In order to constrain the inclination of the system and the mass of the secondary, we can consider also the ellipsoidal deformation of the primary. The amplitude of the ellipsoidal modulation, equal to 368.0 ± 11.7 (section 4.1), is roughly proportional to $\approx (M_2/M_1) (R_1/a)^3 \sin^2 i$, where a is the orbital semi-major axis and R_1 is the radius of the primary. A more detailed treatment is given by Morris & Naftilan (1993).

The radius of the primary can be estimated from $R_1 = (GM_1/g)^{1/2}$, which gives for example $\sim 0.102 R_\odot$ for $M_1 = 0.19 M_\odot$. Using a gravity darkening coefficient of 0.479 ± 0.010 (see section 5.1) and adopting 0.27 ± 0.02 for the linear limb darkening coefficient in the *Kepler* passband (Claret & Bloemen 2011), we can search for the best values of i and M_2 that satisfy equation (3) of Morris & Naftilan (1993). These solutions are shown in Fig. 6 as blue dots. The uncertainties in green or violet (68% confidence) were computed by means of the simpler equation (6) of Morris 1985 (which, in our case, gives results almost identical to Morris & Naftilan 1993, always within 2%), taking into account the observational uncertainties in $\log g$, K_1 , amplitude of the ellipsoidal deformation and orbital period. For the mass of the primary we assumed an indetermination of $\pm 0.02 M_\odot$. Despite the large uncertainties that we see in Fig. 6, the best values that we obtain for M_2 are in good agreement with

⁴ From here on the terms ‘‘primary’’ and ‘‘secondary’’ are used to indicate the brightest (sdB) and the faintest (WD) star of the binary, without any reference to the initially most massive star.

typical WD masses. More importantly, Fig. 6 suggests a relatively low inclination $i \lesssim 40^\circ$, with a maximum probability near 20 degrees. This is true for any primary mass and implies a minimum mass of $\sim 0.2 M_\odot$ for the secondary. The large uncertainties on i and M_2 in Fig. 6 are roughly proportional to the uncertainty in $\log g$, which dominates the error budget. A better determination of the surface gravity would be important to further constrain the system.

5.1 Markov chain Monte Carlo simulations

In order to confirm the analytical results of Fig. 6, and despite the level of degeneracy, we made an attempt to constrain the parameters of the system by modelling the light curve using the LCURVE light curve synthesis code and performing Markov chain Monte Carlo (MCMC) simulations (see Copperwheat et al. 2010 and Bloemen et al. 2011 for details of the code). The gravity and limb darkening coefficients for the primary were computed using the same sdB atmosphere models as used in the computation of the beaming factor (section 4.1), assuming $E(B-V)=0.06$. The gravity darkening coefficient was set to 0.479 ± 0.010 , accounting for the uncertainty in T_{eff} and $\log g$, while the limb darkening coefficient was obtained from a 4-parameter law (eq. (5) of Claret & Bloemen 2011). Then we fixed the RV amplitude of the primary to the spectroscopic value, $K_1 = 97.2 \pm 2$ km/s, and we assumed a WD radius $R_2 = 0.015 \pm 0.003 R_\odot$. Actually this value has a much larger uncertainty (and there are no eclipses that constrain the radii) but this does not affect the results since the light contribution of the white dwarf is only $\sim 0.2\%$. Three MCMC runs were launched with a primary mass of 0.18, 0.24 and 0.36 M_\odot . Inclination, mass ratio and beaming factor were kept as free parameters. The results give an average inclination near 20 degrees, in agreement with the analytical results. Moreover the formal uncertainties indicate an inclination below 50 degrees at a 95% confidence level for all these primary masses. However, these uncertainties are not very reliable because of convergence problems that are due to the very wide allowed range in the inclination and the highly nonlinear relation of the inclination with other parameters such as the mass ratio. From the MCMC simulations we obtained a beaming factor of 1.33 ± 0.03 , confirming that the photometric contamination must be $\sim 12\%$ in order to bring this value to 1.51 ± 0.02 as obtained from synthetic spectra.

5.2 Different scenarios for the sdB evolution

If the mass of KIC 6614501's primary is below $\sim 0.30 M_\odot$, it must be a He-core WD progenitor and we can compare its effective temperature and surface gravity with He-core WD evolutionary tracks. We obtain two possible scenarios: i) for M_1 near 0.18-0.19 M_\odot , T_{eff} and $\log g$ are compatible with a He-core white dwarf already on the final cooling track (after the possible H-shell flashes). In this scenario a higher mass is excluded because the smaller radius due to the electron degeneracy would be incompatible with the surface gravity and with the amplitude of the ellipsoidal deformation. Indeed, looking at Panei et al. (2007), we see that there is only one model that, having already reached the final cooling sequence, can fit T_{eff} and $\log g$ of KIC 6614501's primary: it is the model with a mass of 0.1869 M_\odot between phase C and D, which corresponds to an age of about 180 Myr from the end of the mass transfer. The evolution is still relatively fast and the match between theoretical and observed T_{eff} and $\log g$ is valid only for about 1 Myr.

Masses smaller than $\sim 0.18 M_\odot$ (e.g. Panei et al. (2007)'s model with 0.1604 M_\odot) are ruled out because the star would never reach an effective temperature of 23 700 K. ii) For $M_1 \gtrsim 0.19 M_\odot$, the sdB atmospheric parameters are compatible with a low-mass He-core WD progenitor that has not yet reached the final WD cooling branch and is evolving along one of the cooling sequences related to the H-shell flash episodes. For example T_{eff} and $\log g$ are compatible with the 0.196 M_\odot (fourth cooling branch) or 0.242 M_\odot (first cooling branch) model of Althaus et al. (2001). The agreement between theoretical and observed T_{eff} and $\log g$ is valid for less than 1 Myr or almost 2 Myr, and the age would be, respectively, 290 or only 30 Myr.

If the mass of KIC 6614501's primary is larger than $\sim 0.32 M_\odot$, there is another possibility: iii) the sdB is a He-core burning object belonging to the extreme horizontal branch with a unusually low mass, between ~ 0.32 and $\sim 0.40 M_\odot$. For such low masses the theoretical sdB evolutionary tracks (Han et al. 2002) pass through the position of KIC 6614501's primary in the $T_{\text{eff}}/\log g$ diagram. To explore this possibility we computed a set of zero-age and terminal-age EHB (ZAEHB and TAEHB) for sdB masses of 0.33, 0.40 and 0.47 M_\odot , with different envelope masses (0.00001, 0.0001, 0.001 and 0.005 M_\odot). These ZAEHB and TAEHB tracks are shown in Fig. 7. We see from Fig. 7 that, if the mass of KIC 6614501's primary was close to 0.33 M_\odot , the star would be close to the He-core exhaustion while, for a mass near 0.40 M_\odot , it would be close to the ZAEHB and much younger. Such low-mass EHB stars are created from a progenitor with an initial mass between 2 and 2.5 M_\odot , for which the He-core ignition happens under non-degenerate conditions (Han et al. 2002; Hu et al. 2007; Prada Moroni & Straniero 2009). Usually, sdB stars are considered to be post-He-flash objects and thus having a mass near 0.47 M_\odot . However, binary population synthesis models by Han et al. (2003) show that sdB masses down to 0.32 M_\odot can occur in a close binary with a WD companion through the so-called second common envelope ejection channel. Although these low sdB masses occur less frequently than the canonical 0.47 M_\odot , they should not be neglected.

With the current data it is difficult to say which of the three scenarios proposed, He-core WD, He-core WD progenitor in a H-shell flash loop, or low-mass C/O-core WD progenitor, is the correct one. We note, however, that the first hypothesis implies a secondary mass close to the peak of the WD mass distribution: for $M_1 = 0.19 M_\odot$, we obtain $i = 21.2^\circ \pm 13.5_{-3.7}^5$ and $M_2 = 0.57 \pm 0.26_{-0.36}^{0.26} M_\odot$. An sdB mass greater by a factor of 2 would result in a higher luminosity by the same factor. Thus, to know the distance of KIC 6614501 would help to discriminate between the different possibilities. It is interesting to note that, from one hand, a low-mass EHB star would be compatible also with T_{eff} and $\log g$ of the other two objects close to KIC 6614501's primary in the $T_{\text{eff}}/\log g$ diagram (Fig. 7): HD 188112 and SDSS J1625+3632. But on the other hand, the known trigonometric distance of HD 188112 implies a mass of $0.24 \pm 0.10_{-0.07}^{0.10} M_\odot$ (Heber et al. 2003), which points towards a He-core WD progenitor, although a low-mass EHB of ~ 0.32 -0.34 M_\odot can not be totally excluded.

In all the three scenarios proposed, KIC 6614501 is expected to merge in a time shorter than a Hubble time due to gravitational wave radiation. Following Paczyński (1967), the merging time varies between 0.9 (for $M_1=0.40$ and $M_2=1.01 M_\odot$) and 3.1 Gyr (for $M_1=0.18$ and $M_2=0.54 M_\odot$).

6 KIC 6614501'S PRIMARY IN THE CONTEXT OF HE-CORE WHITE DWARFS

Low-mass white dwarfs have masses below $\sim 0.45 M_{\odot}$ and they are generally thought to contain inert helium cores. However, a carbon/oxygen (C/O) core is not excluded for masses down to $\sim 0.33 M_{\odot}$ (Panei et al. 2007; Prada Moroni & Straniero 2009). Below $0.3 M_{\odot}$, helium burning is ruled out and the white dwarfs must have helium cores. These objects are also called extremely low mass (ELM) white dwarfs. At least for solar metallicities, ELM white dwarfs can form only from binary systems. At higher metallicity it is less clear and the possible detection of single low-mass white dwarfs in NGC 6791, one of the oldest ($\lesssim 8$ Gyr) and most metal-rich ($[\text{Fe}/\text{H}] \approx +0.4$) open clusters of our Galaxy, has prompted a heated debate (Origlia et al. 2006; Kalirai et al. 2007). The evolution of He-core white dwarf models with low- or high-metallicity progenitors has been studied by Serenelli et al. (2002) and Althaus et al. (2009) respectively.

With a mass between ~ 0.18 and $\sim 0.40 M_{\odot}$, the primary star of KIC 6614501 is a precursor of a low-mass white dwarf. If the mass is larger than about $0.32 M_{\odot}$, it may evolve into a low-mass C/O-core white dwarf. For lower masses it will become a He-core WD. If the mass is near 0.18 - $0.19 M_{\odot}$, it may have already reached the final ELM WD cooling sequence.

The ELM white dwarfs (and their precursors)⁵ are a rare class of stars. A list of these post-RGB low-mass objects from the literature is given in Table 4. Actually the list we found was longer but we decided to show only those with a high reliability, for which the orbital period was measured through radial velocities and/or high precision photometry from space (*Kepler*). Moreover, we selected only those with $\log g < 7.0$, which corresponds to exclude those with a mass higher than $0.3 M_{\odot}$ (see Kilic et al. 2011a, Fig. 8). Some new objects recently found by the ELM survey (Brown et al. 2012), which do not meet our criteria, are not in Table 4. Similarly, we have not included the primary star of SDSS J1257+5428 (Marsh et al. 2011) because of the large uncertainties, in particular in $\log g$. In most cases, the masses reported in Table 4 are obtained from evolutionary tracks and hence are model dependent. For example, the evolutionary tracks of Panei et al. (2007) differ from those of Driebe et al. (1998), in particular for what concerns very low masses. Panei et al. (2007) have shown that, when element diffusion is included, a dichotomy appears for stellar masses near $0.17 M_{\odot}$: below this limit, the envelope is thick enough for residual nuclear burning that slows down the evolution. For most systems in Table 4 that have a WD companion, only the minimum mass of the secondary is known and thus a more massive neutron star or black hole companion can not be excluded. The position of the objects of Table 4 in the $T_{\text{eff}}/\log g$ plane is shown in Fig. 7. In this figure we note that KIC 6614501 is the hottest object, in a region of the $T_{\text{eff}}/\log g$ plane that is still quite empty. Only other two stars reside in the same region: HD 188112, at slightly lower T_{eff} , and SDSS J1625+3632 at almost identical T_{eff} but higher gravity. These objects are crucial to study the limit between He-core burning EHB stars, that will become low-mass C/O-core white dwarfs, and He-core WD progenitors. They can be important also to study the complex evolutionary path that, through the H-shell flashes, leads to the formation of He-core (ELM) white dwarfs.

⁵ The difference between ELM WDs and their precursors is subtle. In the next lines we will simply use the term ELM WDs for all of them, according with recent articles.

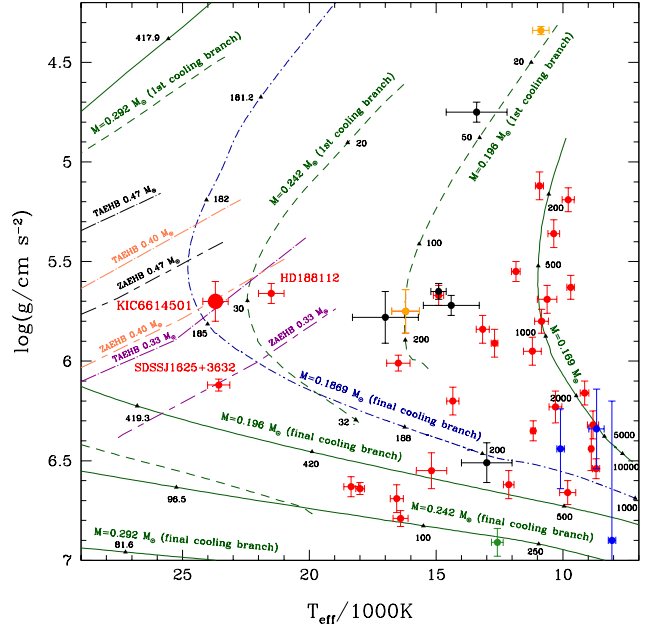


Figure 7. ELM white dwarfs in the $T_{\text{eff}}/\log g$ plane. These objects are in binary systems with a main sequence star, a white dwarf, or a neutron star (black, red, or blue symbols respectively, colors available only in the electronic version). The two objects in yellow are in globular clusters. The green symbol corresponds to SDSS J1448+1342, that could be either the component of a pole-on binary or a single star. More details on the single objects are given in Table 4. The evolutionary tracks are from Althaus et al. (2001), with a mass of 0.169 , 0.196 , 0.242 and $0.292 M_{\odot}$. For the models with a mass greater than $0.17 M_{\odot}$, which experience at least one thermonuclear H-shell flash, we show only the first and the last cooling branch (those with a longer duration and a higher probability to be populated) for clarity. Moreover we have included also the final cooling branch of the $0.1868 M_{\odot}$ model from Panei et al. (2007), which matches very well the atmospheric parameters of KIC 6614501's primary. The numbers close to the triangles are the ages in Myrs from the end of the mass transfer. The ZAEHB and TAEHB tracks for sdB masses of 0.33 , 0.40 and $0.47 M_{\odot}$ are reported and correspond to a range of envelope masses between 0.00001 and $0.005 M_{\odot}$.

ACKNOWLEDGMENTS

The authors thank Conny Aerts and Andrew Tkachenko for the work done in organising and leading the KASC WG9 on binary stars and maintaining its web site, making easier the realisation of this article. They also thank Ronald L. Gilliland, Martin Still and Karen Kinemuchi for useful informations on the *Kepler* pixel data; and the reviewer, Stephan Vennes, for helpful comments on the paper. R.S. was supported by the PRIN-INAF on “Asteroseismology: looking inside the stars with space- and ground-based observations”. R.H.Ø. and S.B. have received support through the European Research Council under the European Community’s Seventh Framework Programme (FP7/2007–2013)/ERC grant agreement N°227224 (PROSPERITY), as well as from the Research Council of K.U. Leuven grant agreement GOA/2008/04. M.D.R. and L.E.F. were supported by the Missouri Space Grant, funded by NASA. P.D. is a Postdoctoral Fellow of the Fund for Scientific Research of Flanders (FWO). H.H. was supported by the Netherlands Organisation for Scientific Research (NWO). T.R.M. was supported by the Science and Technology Facilities Council. Finally, the authors gratefully acknowledge the *Kepler* team and everybody who has

Table 4. ELM white dwarfs.

System name	g mag ^a	T_{eff}/K	$\log(g/\text{cm s}^{-2})$	M_1/M_{\odot}	P_{orb}/d	Ecl. ^b	Comp.	M_2/M_{\odot}	Ref
V209 ω Cen	V=16.58	10866 \pm 323	4.34 \pm 0.02	0.14	0.834	2	reborn WD	0.94	1
WASP J0247–25	V=12.44	13400 \pm 1200	4.75 \pm 0.05	0.23	0.668	2	A-type	1.48	2
SDSS J1233+1602	19.83	10920 \pm 160	5.12 \pm 0.07	0.17	0.151		WD	\geq 0.86	3
SDSS J1741+6526	18.27	9790 \pm 240	5.19 \pm 0.06	0.16	0.061		WD	\geq 1.10	4
SDSS J2119–0018	20.00	10360 \pm 230	5.36 \pm 0.07	0.17	0.087		WD	\geq 0.75	3
SDSS J0917+4638	18.70	11850 \pm 170	5.55 \pm 0.05	0.17	0.316		WD	\geq 0.27	3
SDSS J0112+1835	17.11	9690 \pm 150	5.63 \pm 0.06	0.16	0.147		WD	\geq 0.62	4
KIC 10657664	13.08 ^c	14900 \pm 300 ^d	5.65 \pm 0.04 ^d	0.37 ^d	3.273	2	A-type	2.5	5
HD 188112	V=10.2	21500 \pm 500	5.66 \pm 0.05	0.24	0.607		WD	\geq 0.73	6
GALLEX J1717	V=13.7	14900 \pm 200	5.67 \pm 0.05	0.18	0.246	1	WD	0.9	7
SDSS J0818+3536	20.48	10620 \pm 380	5.69 \pm 0.07	0.17	0.183		WD	\geq 0.26	3
KIC 06614501	15.80 ^c	23700 \pm 500	5.70 \pm 0.10	0.24	0.157	0	WD	\sim 0.5-1.1	8
KOI 1224 ^e	14.01 ^c	14400 \pm 1100	5.72 \pm 0.05	0.20	2.698	2	A/F	1.59	9
NGC 6121 V46	V=18.5	16200 \pm 550	5.75 \pm 0.11	0.19	0.087	0	WD	\geq 0.26	10
KOI 81 ^f	11.30 ^c	17000 \pm 1300	5.78 \pm 0.13	0.3	23.878	2	B9-type	2.7	11
SDSS J0152+0749	18.01	10840 \pm 270	5.80 \pm 0.06	0.17	0.323		WD	\geq 0.57	4
SDSS J0755+4906	20.09	13160 \pm 260	5.84 \pm 0.07	0.17	0.063		WD	\geq 0.81	3
SDSS J1422+4352	19.79	12690 \pm 130	5.91 \pm 0.07	0.17	0.379		WD	\geq 0.41	3
SDSS J1630+2712	20.04	11200 \pm 350	5.95 \pm 0.07	0.17	0.276		WD	\geq 0.52	3
SDSS J0106–1000	19.8	16490 \pm 460	6.01 \pm 0.04	0.17	0.027	0	WD	0.4	12
SDSS J1625+3632	19.36	23570 \pm 440	6.12 \pm 0.03	0.20	0.232		WD	\geq 0.07	13
SDSS J1840+6423	18.76	9140 \pm 170	6.16 \pm 0.06	0.17	0.191		WD	\geq 0.64	4
SDSS J1439+1002	17.81	14340 \pm 240	6.20 \pm 0.07	0.18	0.437		WD	\geq 0.46	3
SDSS J0849+0445	19.31	10290 \pm 250	6.23 \pm 0.08	0.17	0.079		WD	\geq 0.64	14
SDSS J1443+1509	18.58	8810 \pm 220	6.32 \pm 0.07	0.17	0.191		WD	\geq 0.83	4
PSR J1012+5307	V=19.6	8670 \pm 300	6.34 \pm 0.20	0.16	0.605		PSR	1.6	15,16
LP 400-22	V=17.22	11170 \pm 90	6.35 \pm 0.05	0.19	1.010		WD	\geq 0.41	17,18,19
PSR J1911–5958	V=22.1	10090 \pm 150	6.44 \pm 0.20	0.18	0.837		PSR	1.34	20
SDSS J0822+2753	18.33	8880 \pm 60	6.44 \pm 0.11	0.17	0.244		WD	\geq 0.76	14
KOI 74 ^g	10.85 ^c	13000 \pm 1000	6.51 \pm 0.10	0.23	5.189	2	A1-type	2.2	11,21
NLTT 11748	V=16.7 ^h	8690 \pm 140	6.54 \pm 0.05	0.18	0.235	2	WD	0.76	22,23,24,25,26
SDSS J1053+5200	18.93	15180 \pm 600	6.55 \pm 0.09	0.20	0.043		WD	\geq 0.26	14,3
SDSS J1512+2615	19.24	12130 \pm 210	6.62 \pm 0.07	0.20	0.600		WD	\geq 0.28	3
SDSS J0923+3028	15.63	18350 \pm 290	6.63 \pm 0.05	0.23	0.045		WD	\geq 0.34	3
SDSS J1234–0228	17.86	18000 \pm 170 ⁱ	6.64 \pm 0.03 ⁱ	0.23	0.091		WD	\geq 0.09	13
SDSS J1518+0658	17.46	9810 \pm 320	6.66 \pm 0.06	0.20	0.609		WD	\geq 0.58	4
SDSS J1436+5010	18.23	16550 \pm 260	6.69 \pm 0.07	0.24	0.046		WD	\geq 0.46	14
SDSS J0651+2844	19.1	16400 \pm 300	6.79 \pm 0.04	0.25	0.009	2	WD	0.55	27
PSR J0218+4232	V=24.2	8060 \pm 150	6.9 \pm 0.7	0.2	2.029		PSR	1.6	28
SDSS J1448+1342	19.22	12580 \pm 230	6.91 \pm 0.07	0.25	^l				3

Notes: ^a system's magnitude; ^b eclipse: 0=not detected, 1=secondary ecl. detected, 2=secondary and primary ecl. detected; ^c from Kepler Input Catalogue; ^d a secondary solution from the same authors gives $T_{\text{eff}}/K=14600 \pm 300$, $\log g=5.50 \pm 0.02$, $M/M_{\odot}=0.26$; ^e KIC 6606653; ^f KIC 8823868; ^g KIC 6889235; ^h from USNO; ⁱ $T_{\text{eff}}/K=17470 \pm 750$, $\log g=6.38 \pm 0.05$ from Liebert et al. 2004; ^l can be either a pole-on binary or a single ELM WD, see Brown et al. 2010 for more details.

References: 1 Kaluzny et al. 2007, 2 Maxted et al. 2011, 3 Brown et al. 2010, 4 Brown et al. 2012, 5 Carter et al. 2011, 6 Heber et al. 2003, 7 Vennes et al. 2011, 8 this paper, 9 Breton et al. 2012, 10 O'Toole et al. 2006, 11 van Kerkwijk et al. 2010, 12 Kilic et al. 2011b, 13 Kilic et al. 2011a, 14 Kilic et al. 2010a, 15 van Kerkwijk et al. 1996, 16 Callanan et al. 1998, 17 Vennes et al. 2009, 18 Kilic et al. 2009, 19 Kawka et al. 2006, 20 Bassa et al. 2006, 21 Bloemen et al. 2012, 22 Kawka & Vennes 2009, 23 Kawka et al. 2010, 24 Steinfadt et al. 2010, 25 Kilic et al. 2010b, 26 Shporer et al. 2010, 27 Brown et al. 2011, 28 Bassa et al. 2003.

contributed to making this mission possible. Funding for the *Kepler Mission* is provided by NASA's Science Mission Directorate.

REFERENCES

- Althaus L. G., Serenelli A. M., Benvenuto O. G., 2001, MNRAS, 323, 471
- Althaus L. G., Panei J. A., Romero A. D., Rohrmann R. D., Córscico A. H., García-Berro E., Miller Bertolami M. M., 2009, A&A, 502, 207
- Bassa C. G., van Kerkwijk M. H., Kulkarni S. R., 2003, A&A, 403, 1067
- Bassa C. G., van Kerkwijk M. H., Koester D., Verbunt F., 2006, A&A, 456, 295
- Bloemen S. et al., 2011, MNRAS, 410, 1787
- Bloemen S. et al., 2012, MNRAS, in press (arXiv:1202.5553)
- Borucki W. J. et al., 2010, Science, 327, 977

- Breton R. P., Rappaport S. A., van Kerkwijk M. H., Carter J. A., 2012, submitted to ApJ, arXiv:1109.6847
- Brown T. M., Ferguson H. C., Davidsen A. F., Dorman B., 1997, ApJ, 482, 685
- Brown W. R., Kilic M., Allende Prieto C., Kenyon S. J., 2010, ApJ, 723, 1072
- Brown W. R., Kilic M., Hermes J. J., Allende Prieto C., Kenyon S. J., Winget D. E., 2011, ApJ, 737, L23
- Brown W. R., Kilic M., Allende Prieto C., Kenyon S. J., 2012, ApJ, 744, 142
- Callanan P. J., Garnavich P. M., Koester D., 1998, MNRAS, 298, 207
- Carter J. A., Rappaport S., Fabrycky D., 2011, ApJ, 728, 139
- Claret A., Bloemen S., 2011, A&A, 529, 75
- Copperwheat C. M., Marsh T. R., Dhillon V. S., Littlefair S. P., Hickman R., Gänsicke B. T., Southworth J., 2010, MNRAS, 402, 1824
- Copperwheat C. M., Morales-Rueda L., Marsh T. R., Maxted P. F. L., Heber U., 2011, MNRAS, 415, 1381
- Degroote P. et al., 2011, A&A, 536, 82
- Driebe T., Schönberner D., Blöcker T., Herwig F., 1998, A&A, 339, 123
- Geier S., Nesslinger S., Heber U., Przybilla N., Napiwotzki R., Kudritzki R.-P., 2007, A&A, 464, 299
- Geier S. et al., 2011a, A&A, 526, 39
- Geier S. et al., 2011b, A&A, 530, 28
- Gilliland R. L. et al., 2010, PASP, 122, 131
- Greggio L., Renzini A., 1990, ApJ, 364, 35
- Groot P. J. et al., 2009, MNRAS, 399, 323
- Han Z., Podsiadlowski Ph., Maxted P. F. L., Marsch T. R., Ivanova N., 2002, MNRAS, 336, 449
- Han Z., Podsiadlowski Ph., Maxted P. F. L., Marsh T. R., 2003, MNRAS, 341, 669
- Heber U., Reid I. N., Werner K., 2000, A&A, 363, 198
- Heber U., Edlmann H., Lisker T., Napiwotzki R., 2003, A&A, 411, L477
- Heber U., 2009, ARA&A, 47, 211
- Hills J. G., Dale T. M., 1974, A&A, 30, 135
- Hu H., Nelemans G., Østensen R., Aerts C., Vučković M., Groot P. J., 2007, A&A, 473, 569
- Kalirai J. S., Bergeron P., Hansen B. M. S., Kelson D. D., Reitzel D. B., Rich R. M., Richer H. B., 2007, ApJ, 671, 748
- Kaluzny J., Rucinski S. M., Thompson I. B., Pych W., Krzeminski W., 2007, AJ, 133, 2457
- Kawaler S. D. et al., 2010, MNRAS, 409, 1509
- Kawka A., Vennes S., Oswalt T. D., Smith J. A., Silvestri N. M., 2006, ApJ, 643, L123
- Kawka A., Vennes S., 2009, A&A, 506, L25
- Kawka A., Vennes S., Vaccaro T. R., 2010, A&A, 516, L7
- Kilic M., Brown W. R., Allende Prieto C., Swift B., Kenyon S. J., Liebert J., Agüeros M. A., 2009, ApJ, 695, L96
- Kilic M., Brown W. R., Allende Prieto C., Kenyon S. J., Panei J. A., 2010a, ApJ, 716, 122
- Kilic M. et al., 2010b, ApJ, 721, L158
- Kilic M., Brown W. R., Allende Prieto C., Agüeros M. A., Heinke C., Kenyon S. J., 2011a, ApJ, 727, 3
- Kilic M. et al., 2011b, MNRAS, 413, L101
- Koester D., Voss B., Napiwotzki R., Christlieb N., Homeier D., Lisker T., Reimers D., Heber U., 2009, A&A, 505, 441
- Liebert J., Bergeron P., Eisenstein D., Harris H. C., Kleinman S. J., et al., 2004, ApJ, 606, L147
- Loeb A., Gaudi B. S., 2003, ApJ, 588, L117
- Marsh T. R., Gänsicke B. T., Steeghs D., Southworth J., Koester D., Harris V., Merry L., 2011, ApJ, 736, 95
- Maxted P. F. L., Marsh T. R., North R. C., 2000, MNRAS, 317, L41
- Maxted P. F. L., Heber U., Marsh T. R., North R. C., 2001, MNRAS, 326, 1391
- Maxted P. F. L., Anderson D. R., Burleigh M. R. et al., 2011, MNRAS, 418, 1156
- Mazeh T., Faigler S., 2010, A&A, 521, L59
- Morris S. L., 1985, ApJ, 295, 143
- Morris S. L., Naftilan S. A., 1993, ApJ, 419, 344
- Napiwotzki R., Karl C. A., Lisker T., Heber U., Christlieb N., Reimers D., Nelemans G., Homeier D., 2004, Ap&SS Sci., 291, 321
- Origlia L., Valenti E., Rich R. M., Ferraro F. R., 2006, ApJ, 646, 499
- Østensen R. H. et al., 2010a, MNRAS, 408, L51
- Østensen R. H. et al., 2010b, MNRAS, 409, 1470
- Østensen R. H. et al., 2011, MNRAS, 414, 2860
- O'Toole S. J., Napiwotzki R., Heber U., Drechsel H., Frandsen S., Grundahl F., Bruntt H., 2006, Baltic Astronomy, 15, 61
- Paczyński B., 1967, Acta Astronomica, 17, 287
- Panei J. A., Althaus L. G., Chen X., Han Z., 2007, MNRAS, 382, 779
- Prada Moroni P. G., Straniero O., 2009, A&A, 507, 1575
- Serenelli A. M., Althaus L. G., Rohrmann R. D., Benvenuto O. G., 2002, MNRAS, 337, 1091
- Shporer A., Kaplan D. L., Steinfadt J. D. R., Bildsten L., Howell S. B., Mazeh T., 2010, ApJ, 725, L200
- Steinfadt J. D. R., Kaplan D. L., Shporer A., Bildsten L., Howell S. B., 2010, ApJ, 716, L146
- Telting J. H. et al., 2012, A&A, submitted
- van Kerkwijk M. H., Bergeron P., Kulkarni S. R., 1996, ApJ, 467, L89
- van Kerkwijk M. H., Rappaport S. A., Breton R. P., Justham S., Podsiadlowski P., Han Z., 2010, ApJ, 715, 51
- Vennes S., Kawka A., Vaccaro T. R., Silvestri N. M., 2009, A&A, 507, 1613
- Vennes S., Thorstensen J. R., Kawka A. et al., 2011, ApJ, 737, L16
- Zucker S., Mazeh T., Alexander T., 2007, ApJ, 670, 1326